Three-Dimensional Coherent Optical Waves Localized on Trochoidal Parametric Surfaces

T. H. Lu, Y. C. Lin, Y. F. Chen,* and K. F. Huang
Department of Electrophysics, National Chiao Tung University, Hsinchu, Taiwan
(Received 24 June 2008; published 2 December 2008)

We theoretically demonstrate that the three-dimensional (3D) coherent laser waves formed by the degenerate Laguerre-Gaussian modes with different longitudinal indices are well localized on rotating trochoidal parametric surfaces. We further use a large-Fresnel-number laser system to realize the existence of the laser modes related to trochoidal coherent states. Experimental results reveal that the exotic laser modes generally originate from a superposition of two degenerate standing-wave trochoidal coherent states.

DOI: 10.1103/PhysRevLett.101.233901 PACS numbers: 42.60.Jf, 05.45.−a, 42.55.Xi

It is known that the propagation of a coherent optical wave inside a laser resonator is closely similar to the propagation of a quantum wave inside a mesoscopic structure [1]. This profound similarity has been growingly employed to realize many quantum signatures in optical context, such as quantum chaos phenomena [2], disorder induced wave localization [3], geometric phases [4], and the issue of quantum tunneling [5]. Recently, various laser systems have been widely used to study optical pattern formation including the Laguerre-Gaussian modes, Hermite-Gaussian modes, and the generalized coherent states that form a general family to comprise the Hermite-Gaussian and Laguerre-Gaussian mode families as special cases [6,7].

In modern physics, classical orbits have been found to play a critical role in explaining carriers transport in ballistic mesoscopic structures [8] and oscillations in the photodetachment cross sections [9]. The Hermite-Gaussian modes are identical to the eigenstates of a two-dimensional (2D) harmonic oscillator [10]; the related classical periodic orbits are the Lissajous figures. On the other hand, the Laguerre-Gaussian modes can correspond to the eigenstates of a charged particle in crossed electric and magnetic fields [11]; the classical periodic orbits are the trochoids that include cycloids, epicycloids, hypocycloids, cardioids, etc. By definition, a trochoid is a roulette given by rolling a circle on or in a second circle. Trochoidal orbits are ubiquitous in nature such as in planetary dynamics [12], ocean waves [13], Belousov-Zhabotinsky reactions [14], and crank-and-slider mechanism. Although laser resonators have been successfully employed to illustrate the correspondence between quantum wave functions and classical Lissajous orbits [15], there has been no study with regard to the laser modes related to the trochoidal orbits thus far.

In this Letter we originally verify that the coherent superposition of the degenerate Laguerre-Gaussian laser modes with different longitudinal indices leads to the formation of three-dimensional (3D) coherent states concentrated on rotating trochoidal parametric surfaces. With the quantum-classical isomorphism, the trochoidal coherent states are derived to be a canonical transformation of the Lissajous coherent states. Furthermore, we experimentally employ a large-Fresnel-number laser system to generate the laser modes related to the trochoidal coherent waves. Since the laser cavity is an excellent analog system for studying the coherent waves, the present findings will be useful for understanding the fundamental behavior of wave functions at the border of the classical and quantum regimes.

First of all, we verify that the longitudinal-transverse coupling in spherical laser cavities can bring about the 3D coherent waves to be localized on rotating trochoidal parametric surfaces. The wave function of Laguerre-Gaussian mode with longitudinal index l, transverse radial index $\tilde{n}$, and transverse azimuthal index $\tilde{m}$ in cylindrical coordinates $(\rho,\ \phi,\ z)$ is given by [10] $\Phi^{(\mathrm{LG})}_{\tilde{n},\tilde{m},l}(\rho,\phi,z) = \Phi^{(\mathrm{LG})}_{\tilde{n},\tilde{m}}(\rho,\phi,z)e^{i(2\tilde{n}+|\tilde{m}|+1)\theta_G(z)}e^{-i\zeta_{\tilde{n},\tilde{m},l}(\rho,z)}$, where

$$\Phi^{(\mathrm{LG})}_{\tilde{n},\tilde{m}}(\rho,\phi,z) = \sqrt{\frac{2\tilde{n}!}{\pi(\tilde{n}+|\tilde{m}|)!}}\frac{1}{w(z)} \times \left(\frac{\sqrt{2}\rho}{w(z)}\right)^{|\tilde{m}|} e^{i\tilde{m}\phi} L^{|\tilde{m}|}_{\tilde{n}}\left(\frac{2\rho^2}{w(z)^2}\right) e^{-\rho^2/w(z)^2}, \tag{1}$$

$w(z) = w_0\sqrt{1+(z/z_R)^2}$, $\zeta_{\tilde{n},\tilde{m},l}(\rho,z) = k_{\tilde{n},\tilde{m},l}z[1+\rho^2/2(z^2+z_R^2)]$, w_0 is the beam radius at the waist, and $z_R = \pi w_0^2/\lambda$ is the Rayleigh range, $L^l_p(\cdot)$ are the associated Laguerre polynomials, $k_{\tilde{n},\tilde{m},l}$ is the wave number, and $\theta_G(z) = \tan^{-1}(z/z_R)$ is the Gouy phase. In terms of the effective length L, the wave number $k_{\tilde{n},\tilde{m},l}$ is given by $k_{\tilde{n},\tilde{m},l}L = \pi[l+(2\tilde{n}+|\tilde{m}|)(\Delta f_T/\Delta f_L)]$, where $\Delta f_L = c/2L$ is the longitudinal mode spacing and Δf_T is the transverse mode spacing. It has been evidenced [15] that when the ratio $\Delta f_T/\Delta f_L$ is close to a simple fractional, the longitudinal-transverse coupling usually leads to the frequency locking among different transverse modes with the help of different longitudinal orders. Consequently, when the mode-spacing ratio $\Delta f_T/\Delta f_L$ is locked to a rational

number P/Q, the group of the Laguerre-Gaussian modes $\Phi^{(\mathrm{LG})}_{\tilde{n}_0+\tilde{p}k,\tilde{m}_0+\tilde{q}k,l_0+sk}$ with $k = 0, 1, 2, 3, \ldots$ can be found to constitute a family of frequency degenerate states, provided that the given integers $(\tilde{p}, \tilde{q}, s)$ obey the equation $s + (2\tilde{p} + \tilde{q})(P/Q) = 0$. For convenience, the integer s is taken to be negative. The equation $s + (2\tilde{p} + \tilde{q})(P/Q) = 0$ indicates that $2\tilde{p} + \tilde{q}$ needs to be an integral multiple of Q, i.e., $2\tilde{p} + \tilde{q} = KQ$, where $K = 1, 2, 3, \ldots$.

With the coherent-state representation [15,16], the 3D coherent wave formed by the family of the degenerated Laguerre-Gaussian modes $\Phi^{(\mathrm{LG})}_{\tilde{n}_0+\tilde{p}k,\tilde{m}_0+\tilde{q}k,l_0+sk}$ can be expressed as $|\Theta^{\tilde{p},\tilde{q},s}_{\tilde{n}_0,\tilde{m}_0,l_0}(\phi_0)\rangle = \sum_{k=-M}^{M} C_{M,k} e^{ik\phi_0} |\Phi^{(\mathrm{LG})}_{\tilde{n}_0+\tilde{p}k,\tilde{m}_0+\tilde{q}k,l_0+sk}\rangle$, where $C_{M,k} = 2^{-M}\binom{2M}{M+k}^{1/2}$ is the weighting coefficient, $\binom{n}{k} = \frac{n!}{k!(n-k)!}$ represents the binomial coefficient, the parameter ϕ_0 is the relative phase between various Laguerre-Gaussian modes at $z = 0$. The weighting coefficients $C_{M,k}$ come from the representation of the quantum spin coherent states [16] that makes the wave functions have the classical picture of the minimum uncertainty for a fixed value of M. In a large-Fresnel-number laser cavity, the resultant field structure with the minimum mode volume can have the lowest lasing threshold to break into oscillation at first. The mode volume is correlated to the localization degree of the wave function. More importantly, the 3D coherent states formed by the degenerate modes with different longitudinal indices have smaller mode volumes than the 2D coherent states formed by the degenerate modes with the same longitudinal index. With the expression of Eq. (1), the 3D coherent state can be rewritten as

$$|\Theta^{\tilde{p},\tilde{q},s}_{\tilde{n}_0,\tilde{m}_0,l_0}(\phi_0)\rangle = |\Theta^{\tilde{p},\tilde{q}}_{\tilde{n}_0,\tilde{m}_0}(\phi_0)\rangle e^{i(2\tilde{n}_0+|\tilde{m}_0|+1)\theta_G(z)} e^{-i\zeta_{\tilde{n}_0,\tilde{m}_0,l_0}(\rho,z)} \tag{2}$$

with

$$|\Theta^{\tilde{p},\tilde{q}}_{\tilde{n}_0,\tilde{m}_0}(\phi_0)\rangle = \sum_{k=-M}^{M} C_{M,k} e^{ik\varphi(z)} e^{ik\phi_0} |\Phi^{(\mathrm{LG})}_{\tilde{n}_0+\tilde{p}k,\tilde{m}_0,\tilde{q}k}\rangle, \tag{3}$$

where $\varphi(z) = (2\tilde{p} + \tilde{q})\theta_G(z)$. Equation (2) indicates that the transverse pattern of the 3D coherent wave is utterly determined by the wave function $\langle x, y, z|\Theta^{\tilde{p},\tilde{q}}_{\tilde{n}_0,\tilde{m}_0}(\phi_0)\rangle$.

Since the Hermite-Gaussian modes of the laser resonator are isomorphic to the eigenstates of the 2D quantum harmonic oscillator, we can use the quantum operator algebra of the harmonic oscillator to deduce the subtle relationship between the Hermite-Gaussian and Laguerre-Gaussian coherent states. With an unitary operator $\hat{U}$ in the Schwinger representation of the SU(2) algebra, the Laguerre-Gaussian mode can be expressed as

$$\begin{aligned} |\Phi^{(\mathrm{LG})}_{\tilde{n},\tilde{m}}\rangle &= \hat{U}|\Phi^{(\mathrm{HG})}_{\tilde{n},N-\tilde{n}}\rangle \\ &= \sum_{K=0}^{N} e^{-iK\pi/2} d^{N/2}_{K-(N/2),\tilde{m}/2}(\pi/2)|\Phi^{(\mathrm{HG})}_{K,N-K}\rangle \end{aligned} \tag{4}$$

with

$$\begin{aligned} \Phi^{(\mathrm{HG})}_{n,m}(x, y, z) &= \frac{1}{\sqrt{2^{m+n-1}\pi m! n!}} \\ &\times \frac{1}{w(z)} H_n\left(\frac{\sqrt{2}x}{w(z)}\right) H_m\left(\frac{\sqrt{2}y}{w(z)}\right) e^{-\rho^2/w(z)^2}, \end{aligned} \tag{5}$$

where $H_n(\cdot)$ are the Hermite polynomials, $N = 2\tilde{n} + |\tilde{m}|$, and $d^{j}_{m',m}(\beta)$ is the well-known Wigner d coefficients. With the relation $|\Phi^{(\mathrm{LG})}_{\tilde{n},\tilde{m}}\rangle = \hat{U}|\Phi^{(\mathrm{HG})}_{\tilde{n},N-\tilde{n}}\rangle$, we have $|\Theta^{\tilde{p},\tilde{q}}_{\tilde{n}_0,\tilde{m}_0}(\phi_0)\rangle = \hat{U}|\Psi^{p,q}_{n_0,m_0}(\phi_0)\rangle$, where $|\Psi^{p,q}_{n_0,m_0}(\phi_0)\rangle = \sum_{k=-M}^{M} C_{M,k} e^{ik\varphi(z)} e^{ik\phi_0} |\Phi^{(\mathrm{HG})}_{n_0+pk,m_0+qk}\rangle$ is the Hermite-Gaussian coherent state, $n_0 = \tilde{n}_0$, $m_0 = \tilde{n}_0 + |\tilde{m}_0|$, $p = \tilde{p}$, and $q = \tilde{p} + \tilde{q}$. The state $|\Psi^{p,q}_{n_0,m_0}(\phi_0)\rangle$ has been verified to have the intensity localized on the Lissajous parametric surface: $x = \mathrm{Re}[X(\vartheta, z)]$; $y = \mathrm{Re}[Y(\vartheta, z)]$, where $0 \le \vartheta \le 2\pi$, $-\infty \le z \le \infty$, $X(\vartheta, z) = \sqrt{n_0} w(z) e^{i[q\vartheta+(\varphi(z)+\phi_0/p)]}$, and $Y(\vartheta, z) = \sqrt{m_0} w(z) e^{ip\vartheta}$ [15]. To be precise, the Lissajous parametric surface is formed by the Lissajous curves with the phase factor varying with the position z. Using the correspondence between classical canonical transform and quantum unitary transform [17] and the isomorphic relation between SU(2) algebra and SO(3) algebra, we can deduce the Laguerre-Gaussian coherent state $|\Theta^{\tilde{p},\tilde{q}}_{\tilde{n}_0,\tilde{m}_0}(\phi_0)\rangle$ to be exactly localized on the parametric surface: $x = \mathrm{Re}[\tilde{X}(\vartheta, z)]$; $y = \mathrm{Re}[\tilde{Y}(\vartheta, z)]$, where

$$\begin{bmatrix} \tilde{X}(\vartheta, z) \\ \tilde{Y}(\vartheta, z) \end{bmatrix} = \frac{1}{\sqrt{2}} \begin{bmatrix} e^{-i(\pi/4)} & -e^{-i(\pi/4)} \\ e^{i(\pi/4)} & e^{i(\pi/4)} \end{bmatrix} \begin{bmatrix} X(\vartheta, z) \\ Y(\vartheta, z) \end{bmatrix}. \tag{6}$$

It can be easily found that the parametric surfaces in Eq. (6) have the transverse patterns to be the trochoidal curves rotating with the position z; therefore, we call these surfaces the trochoidal parametric surfaces. Following the quantum-classical isomorphism, the trochoidal parametric surface can be pictured as a canonical transformation of the Lissajous parametric surface. Figure 1 shows an example to make a comparison between the Lissajous and trochoidal parametric surfaces in the range from $\varphi(z) = -2\pi$ to $\varphi(z) = 2\pi$ with $(\tilde{p}, \tilde{q}) = (-1, 9)$, $P/Q = 2/7$, and $\phi_0 = 0$. Figure 2 depicts four typical numerical transverse patterns for the coherent states $|\Theta^{\tilde{p},\tilde{q}}_{\tilde{n}_0,\tilde{m}_0}(\phi_0)\rangle$ at $z = 0$ with different $(\tilde{p}, \tilde{q})$ and $(\tilde{n}_0, \tilde{m}_0)$. The choice of $M = 3$ in the

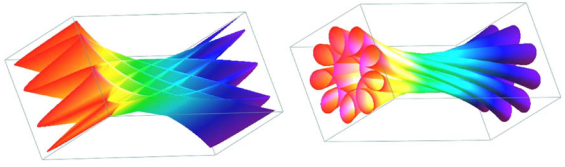

FIG. 1 (color online). Lissajous (left plot) and trochoidal (right plot) parametric surfaces for the 3D coherent waves in the range from $\varphi(z) = -2\pi$ to $\varphi(z) = 2\pi$ with $(\tilde{p}, \tilde{q}) = (-1, 9)$, $(\tilde{n}_0, \tilde{m}_0) = (30, 100)$, $P/Q = 2/7$, and $\phi_0 = 0$.

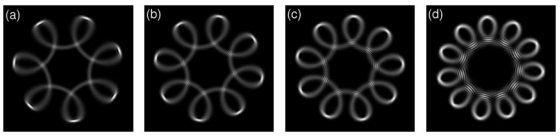

FIG. 2. Numerical transverse patterns for the coherent states $|\Theta^{\tilde{p},\tilde{q}}_{\tilde{n}_0,\tilde{m}_0}(\phi_0)\rangle$ at $z = 0$ with $M = 3$ and $\phi_0 = 0$: (a) $(\tilde{p}, \tilde{q}) = (-1, 7)$ and $(\tilde{n}_0, \tilde{m}_0) = (25, 105)$; (b) $(\tilde{p}, \tilde{q}) = (-1, 8)$ and $(\tilde{n}_0, \tilde{m}_0) = (23, 107)$; (c) $(\tilde{p}, \tilde{q}) = (-1, 9)$ and $(\tilde{n}_0, \tilde{m}_0) = (20, 110)$; (d) $(\tilde{p}, \tilde{q}) = (-1, 11)$ and $(\tilde{n}_0, \tilde{m}_0) = (14, 116)$.

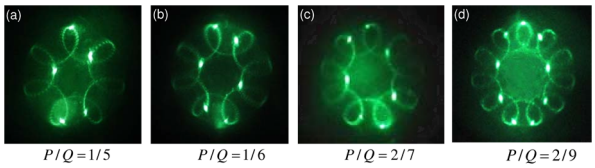

FIG. 3 (color online). Experimental transverse patterns observed at the beam waist $z = 0$ in different cavity lengths: (a) $P/Q = 1/5$; (b) $P/Q = 1/6$; (c) $P/Q = 2/7$; (d) $P/Q = 2/9$.

calculation is just for convenience of presentation because the spatial morphologies of the coherent states can be numerically verified to be strongly concentrated on the trochoidal parametric surfaces as long as $M \geq 2$.

Although we have discovered the 3D coherent waves localized on the Lissajous parametric surfaces in our prior laser experiment with the off-axis pumping scheme [15], the coherent waves related to the trochoidal parametric surfaces were not observed. Recently, we performed systematic experiments and found that the trochoidal coherent waves could be simultaneously generated by exciting the orthogonally polarized Herriott-type nonplanar geometric modes [18]. The Herriott-type nonplanar modes have elliptical patterns of spots in the transverse plane. We experimentally found that these nonplanar geometric modes could be generated in a laser with the transverse orders approximately higher than 1500. Here we use a a-cut 2.0 at. % Nd:YVO_4 crystal with the length of 2 mm and the cross section of 8×8 mm^2 to comply with the requirement of the extremely high transverse orders. The cavity configuration is the same as in Ref. [19]. A microscope objective lens mounted on a translation stage was employed to reimage the tomographic transverse patterns onto a CCD camera. To measure the far-field pattern, the laser output was directly projected on a screen at a distance of ~50 cm from the cavity and the scattered light was captured by a digital camera.

We experimentally find that more than 110 different laser modes related to distinct 3D trochoidal coherent waves can be generated with the degenerate cavities in the range of $1/6 \leq P/Q \leq 1/3$. Figures 3(a)–3(d) show four typical experimental transverse patterns observed at the beam waist $z = 0$ in different cavity lengths. The manifestation of nearly perfect trochoidal curves confirms the laser modes to be associated with the trochoidal coherent waves. On the other hand, the bright spots on each pattern correspond to the Herriott-type mode. Although the polarizations of the trochoidal laser mode and the Herriott-type mode are found to be mutually orthogonal, the Herriott-type mode cannot be removed with an intracavity polarizer because the insertion loss will cause the laser to stop lasing. Nevertheless, an external polarizer can be used to measure the tomographic transverse patterns of the trochoidal laser modes.

It is known that there is a tendency for mutual repulsion of the frequencies for the low-order modes in class-B lasers [20]. As a result, it is important to verify whether the trochoidal laser modes are operated in the single-frequency oscillation or not. The optical spectral information of the laser is monitored by an optical spectrum analyzer (Advantest Q8347) with a resolution of 0.003 nm. Since the transverse mode spacing of the cavity is approximately 0.025 nm, the optical spectrum can be clearly resolved. We measured the optical spectra of the trochoidal laser modes and confirmed these modes to be in the single-frequency oscillation. Moreover, the power spectra of the trochoidal laser modes were also detected and did not reveal any dynamics. In other words, the trochoidal laser modes are indeed stationary states.

Even though the transverse patterns of the trochoidal laser modes at $z = 0$ display precise trochoidal curves, the propagation-varying transverse patterns are observed to be more complicated than a rotating trochoidal wave. Experimental results reveal that the laser modes are associated with the standing-wave trochoidal coherent states. The coherent state $|\Theta^{\tilde{p},\tilde{q}}_{\tilde{n}_0,\tilde{m}_0}(\phi_0)\rangle$ in Eq. (3) behaves as a traveling wave in the transverse plane. The standing-wave representation is expressed as $|S^{\tilde{p},\tilde{q}}_{\tilde{n}_0,\tilde{m}_0}(\phi_0)\rangle = \sum_{k=-M}^{M} C_{M,k} e^{ik\varphi(z)} |\Xi^{\tilde{p},\tilde{q}}_{\tilde{n}_0,\tilde{m}_0}(k, \phi_0)\rangle$, where $|\Xi^{\tilde{p},\tilde{q}}_{\tilde{n}_0,\tilde{m}_0}(k, \phi_0)\rangle = \mathrm{Re}[e^{ik\phi_0} |\Phi^{(\mathrm{LG})}_{\tilde{n}_0+\tilde{p}k,\tilde{m}_0+\tilde{q}k}\rangle]$. Figure 4 shows the numerical results for the tomographic transverse patterns of $|S^{\tilde{p},\tilde{q}}_{\tilde{n}_0,\tilde{m}_0}(\phi_0)\rangle$. To be precise, a standing-wave trochoidal coherent state consists of two trochoidal transverse waves

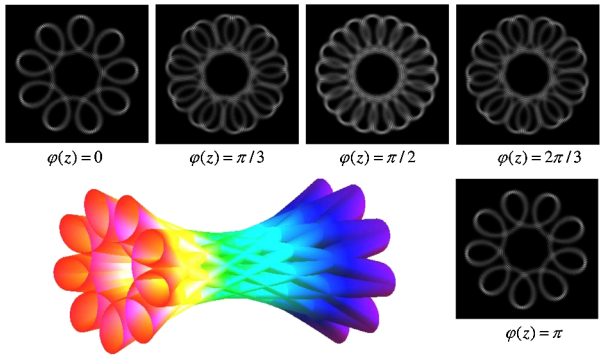

FIG. 4 (color online). Numerical results for the tomographic transverse patterns of the coherent state $|S^{\tilde{p},\tilde{q}}_{\tilde{n}_0,\tilde{m}_0}(\phi_0)\rangle$ with $(\tilde{p}, \tilde{q}) = (-1, 9)$, $(\tilde{n}_0, \tilde{m}_0) = (30, 100)$, $M = 3$, $P/Q = 2/7$, and $\phi_0 = 0$. Parametric-surface plot for illustrating the 3D localization.

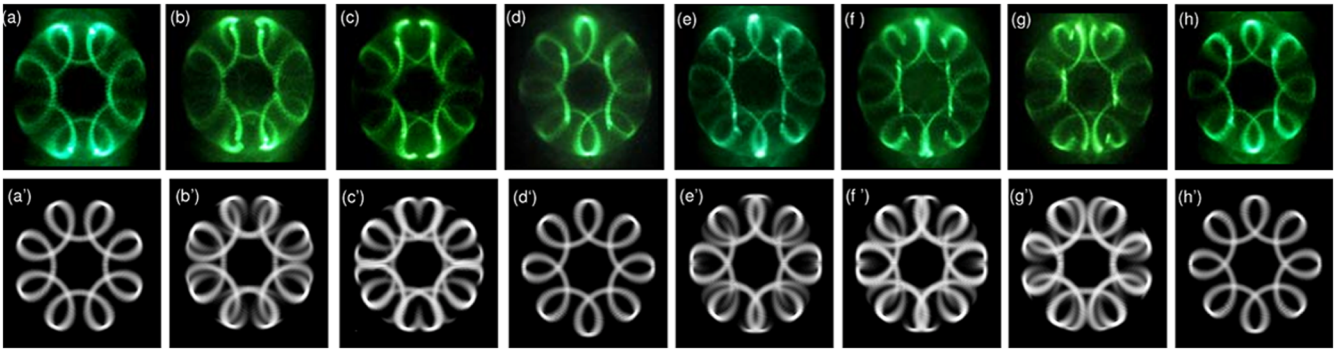

FIG. 5 (color online). (a′)–(h′) Numerical transverse patterns calculated with Eq. (7) and the parameters of $(\tilde{p}, \tilde{q}) = (-1, 8)$, $(\tilde{n}_0, \tilde{m}_0) = (25, 115)$, $M = 3$, and $\phi_0 = -\pi/2$. (a)–(h): Experimental transverse patterns observed in the cavity length with $P/Q = 1/6$. (a) $z = 0L$, (b) $z = 0.23L$, (c) $z = 0.46L$, (d) $z = 1.0L$, (e) $z = 1.33L$, (f) $z = 1.45L$, (g) $z = 2.25L$, (h) far-field region.

rotating in the opposite direction. A parametric-surface plot is also shown in Fig. 4 for illustrating the localization. It is worth noting that the traveling-wave trochoidal coherent states $|\Theta^{\tilde{p},\tilde{q}}_{\tilde{n}_0,\tilde{m}_0}(\phi_0)\rangle$ have an angular momentum of $\tilde{m}_0\hbar$ as the Laguerre-Gaussian modes $|\Phi^{(\mathrm{LG})}_{\tilde{n}_0,\tilde{m}_0}\rangle$ possess, while the standing-wave trochoidal coherent states $|S^{\tilde{p},\tilde{q}}_{\tilde{n}_0,\tilde{m}_0}(\phi_0)\rangle$ have no angular momentum.

Based on thorough experiments and numerical analyses, we discover that the experimental trochoidal waves can be analytically expressed as a quadrature superposition of two degenerate standing-wave trochoidal coherent states:

$$|E\rangle = |S^{\tilde{p},\tilde{q}}_{\tilde{n}_0,\tilde{m}_0}(\phi_0)\rangle + i|S^{\tilde{p},\tilde{q}}_{\tilde{n}_0+1,\tilde{m}_0-2}(\phi_0)\rangle. \quad (7)$$

Note that the experimental transverse orders $\tilde{n}_0$ and $\tilde{m}_0$ exceed 1500; however, the numerical transverse orders are limited to approximately 150 due to a numeric overflow. Even so, the spatial features of the trochoidal coherent waves are generally independent of the transverse indices $\tilde{n}_0$ and $\tilde{m}_0$ for a given $(\tilde{p}, \tilde{q}, \phi_0)$. Therefore, we use lower transverse orders in the calculation to compare with the experimental results. Figures 5(a′)–5(h′) illustrate the numerical transverse patterns calculated with Eq. (7) and the parameters of $(\tilde{p}, \tilde{q}) = (-1, 8)$, $(\tilde{n}_0, \tilde{m}_0) = (25, 115)$, $M = 3$, and $\phi_0 = -\pi/2$. It can be seen that the theoretical features agree very well with the experimental results shown in Figs. 5(a)–5(h). Note that Figs. 5(h) and 5(h′) correspond to the far-field patterns and the same patterns have appeared at $z = L$ shown in Figs. 5(d) and 5(d′).

In summary, we have theoretically demonstrated that the coherent superposition of the degenerate Laguerre-Gaussian modes with different longitudinal indices generates a kind of 3D coherent waves with localization on rotating trochoidal parametric surfaces. Moreover, we have employed a large-Fresnel-number laser resonator to confirm the existence of 3D trochoidal coherent waves. The experimental laser modes are found to come from a superposition of two degenerate standing-wave trochoidal coherent states.

This work is supported by the National Science Council of Taiwan (Contract No. NSC-94-2112-M-009-034).

*yfchen@cc.nctu.edu.tw

[1] A. E. Kaplan *et al.*, Phys. Rev. A **61**, 032101 (2000).
[2] T. Gensty *et al.*, Phys. Rev. Lett. **94**, 233901 (2005); K. F. Huang *et al.*, Phys. Rev. Lett. **89**, 224102 (2002).
[3] Y. F. Chen *et al.*, Phys. Rev. Lett. **96**, 033905 (2006).
[4] E. J. Galvez *et al.*, Phys. Rev. Lett. **90**, 203901 (2003).
[5] I. Vorobeichik *et al.*, Phys. Rev. Lett. **90**, 176806 (2003).
[6] M. Brambilla *et al.*, Phys. Rev. A **43**, 5090 (1991); D. Dangoisse *et al.*, Phys. Rev. A **46**, 5955 (1992); F. Encinas-Sanz, S. Melle, and O. G. Calderon, Phys. Rev. Lett. **93**, 213904 (2004).
[7] S. Danakas and P. K. Aravind, Phys. Rev. A **45**, 1973 (1992).
[8] R. Brunner *et al.*, Phys. Rev. Lett. **98**, 204101 (2007); K. J. Friedland *et al.*, Phys. Rev. B **75**, 045347 (2007); I. V. Zozoulenko and K. F. Berggren, Phys. Rev. B **56**, 6931 (1997).
[9] A. D. Peters, C. Jaffe, and J. B. Delos, Phys. Rev. Lett. **73**, 2825 (1994); C. Bracher and J. B. Delos, Phys. Rev. Lett. **96**, 100404 (2006).
[10] G. Nienhuis and L. Allen, Phys. Rev. A **48**, 656 (1993).
[11] B. L. Johnson and G. Kirczenow, Europhys. Lett. **51**, 367 (2000); P. K. Bhaduri *et al.*, J. Phys. A **27**, L553 (1994).
[12] J. Binney and S. Tremaine, *Galactic Dynamics* (Princeton University Press, Princeton, New Jersey, 1987).
[13] G. Greenhill, Proc. R. Soc. A **94**, 238 (1918).
[14] G. Li *et al.*, Phys. Rev. Lett. **77**, 2105 (1996); B. Sandstede and A. Scheel, Phys. Rev. Lett. **86**, 171 (2001).
[15] Y. F. Chen *et al.*, Phys. Rev. Lett. **96**, 213902 (2006).
[16] M. S. Kumar and B. Dutta-Roy, J. Phys. A **41**, 075306 (2008).
[17] P. A. M. Dirac, *The Principle of Qunatum Mechanics* (Oxford University Press, Oxford, 1958), 4th ed.
[18] D. Herriott, H. Kogelnik, and R. Kompfiier, Appl. Opt. **3**, 523 (1964); I. A. Ramsay and J. J. Degnan, Appl. Opt. **9**, 385 (1970).
[19] T. H. Lu, Y. F. Chen, and K. F. Huang, Phys. Rev. E **75**, 026614 (2007).
[20] K. Staliunas, M. F. H. Tarroja, and C. O. Weiss, Opt. Commun. **102**, 69 (1993); F. Prati, L. Zucchetti, and G. Molteni, Phys. Rev. A **51**, 4093 (1995).